Journal of
Nanoscience and Nanotechnology
Vol. 7, 2647–2653, 2007

Polymer Magnetic Microactuators Fabricated with Hot Embossing and Layer-by-Layer Nano Self-Assembly

Wei Xue and Tianhong Cui*

Department of Mechanical Engineering, University of Minnesota, Minneapolis, MN 55455, USA

Polymer-based magnetic microactuators have been fabricated with hot embossing technique and layer-by-layer (LbL) nano self-assembly. Silicon molds are fabricated with conventional UV lithography and wet etching techniques. Hot embossing is used to transfer the patterns from silicon molds to polymethylmethacrylate (PMMA) sheets. The overall processing time for the pattern transfer is less than 20 min. Low-cost devices with massive and rapid replication can be fabricated. Six layers of magnetic iron oxide (Fe_2O_3) nanoparticles are LbL self-assembled on the PMMA surface as the magnetically sensitive material. Positive photoresist PR1813 is used as the sacrificial layer to protect the gold electrode on the back side of the membrane. LbL nano self-assembly technique provides a simple method to obtain the magnetic film with low cost, short processing time, simple fabrication steps at room temperature. The volume of the magnetic material can be precisely controlled by the number of nano-assembled iron oxide layers. The mechanical, electrical, and magnetic properties of the microactuator are characterized by a laser interferometer. The natural frequency of the actuator is approximately 151 Hz; and the maximum deflection amplitude is about 34 nm. At all frequencies, the increase of the magnetic field increases the deflection amplitude which is in agreement with the theoretical equation.

Keywords: Polymer Magnetic Microactuator, Hot Embossing, Layer-by-Layer (LbL) Nano Self-Assembly, Nanoparticle, Multilayer.

1. INTRODUCTION

Magnetic microactuators have been studied and developed by many research groups.[1, 2] Both soft magnetic materials[3, 4] and hard magnetic materials[5, 6] have been used in the magnetic microactuators. Compared with the electrostatic microactuators, magnetic microactuators have roughly the equivalent efficiency. However, the electromagnetic forces generated by the magnetic microactuators can be much larger than the electrostatic forces generated by the electrostatic microactuators.[7] Therefore, magnetic microactuators can be used in a variety of actuation applications.

Recently, polymer-based magnetic devices have gained a broad theoretical interest and practical applications. A number of polymer-based magnetic microactuators have been developed and fabricated.[8, 9] Due to the advantages of polymer materials such as inexpensive, transparent, flexible, chemically and biologically compatible, and easy to process, polymers can be appealing alternatives to silicon and glass for sensor technologies. For example, the price of a PMMA sheet is about $0.10 per square inch, which is ten times less than silicon wafers. Presently, research work about polymer MEMS, electronics and integrated circuits (ICs) are growing rapidly. It is believed that polymer devices will take the place of silicon devices on low-end applications in the future. The ultimate goal is to integrate polymer mechanical structures and electrical circuit onto a single polymer chip. Low-cost microfabrication techniques and high-volume production can benefit the commercialization of microsystems. Polymers and polymer-based fabrication techniques provide such a space for improvement. Among all polymer microfabrication techniques, hot embossing lithography (HEL), also known as nanoimprint lithography (NIL), has gained broad interest, in particular as a low-cost and high-volume fabrication method to define micro to nanometer scale structures.[10, 11] Hot embossing is suitable for mass production, and does not require special clean-room environment and high-temperature processes. Hot embossing ensures highly precise molding of almost any structures in polymers.

Layer-by-layer (LbL) nano self-assembly of ultrathin films through alternate adsorption of oppositely charged polyions and nanoparticles is an effective and economic approach to build well-organized multilayers in nanometer scale.[12, 13] Due to its versatility and simplicity, LbL self-assembly has gained more and more interest. LbL thin

*Author to whom correspondence should be addressed.

films can be assembled on the surface of almost any materials, such as silicon wafers, plastics, fiber optics, etc.

We designed and developed electron magnetic sensors based on electron tunneling phenomenon. Due to the exponential relationship between the tunneling current and the tunneling gap, tunneling magnetic sensors are able to achieve high sensitivity and high resolution easily.[14] In this paper, we focus on the fabrication and characterization of the polymer-based magnetic microactuators. The devices are fabricated with hot embossing technique and LbL self-assembly. Instead of silicon, an amorphous polymer, polymethylmethacrylate (PMMA), is used as the mechanical material. All the silicon molds are fabricated by conventional bulk-silicon micromachining techniques such as UV lithography and wet etching. Hot embossing is used to transfer the patterns from silicon molds to PMMA.[15] Using the well-developed silicon molds with sharp angles and smooth surfaces, the PMMA structures can be easily replicated within 20 min. The magnetic layers are coated on the PMMA membrane with LbL self-assembly. The self-assembled nanoparticle multilayer is formed with poly(dimethyldiallylammonium chloride) (PDDA), poly(sodium 4-styrenesulfonate) (PSS), and iron oxide (Fe_2O_3) particles. A layer of positive photoresist (PR1813) is used as the sacrificial layer to protect the gold electrode on the membrane. The polymer microactuator is measured as an electrostatic actuator and also an electromagnetic actuator. The measured results of the microactuator are illustrated and discussed in the paper.

2. EXPERIMENAL DETAILS

2.1. Structure and Material

The cross-section schematic of the polymer magnetic microactuator is illustrated in Figure 1. The actuator is designed for electron tunneling magnetic sensor. A PMMA structure with a sharp tunneling tip is used as the substrate. Ti/Au films are deposited and patterned as the tunneling tip electrode and the deflection electrode. Another PMMA structure with a thin membrane is mounted on the substrate. Nanoparticle multilayer including poly(dimethyldiallylammonium chloride) (PDDA), poly (sodium 4-styrenesulfonate) (PSS), and iron oxide (Fe_2O_3) nanoparticles is LbL self-assembled on one side of the membrane. Iron oxide nanoparticles serve as the magnetically sensitive material. On the other side of the membrane, Ti/Au films are sputtered and patterned as the membrane electrode. Two PMMA components are bonded together using conductive epoxy. A feedback control system is used to collect the input signals and provide the control signals to the sensor. When a deflection voltage is applied on the deflection electrode, the membrane is attracted and bends downward due to the electrostatic force established between the deflection electrode and the membrane electrode. Through changing the voltage, the distance of the gap can be controlled.

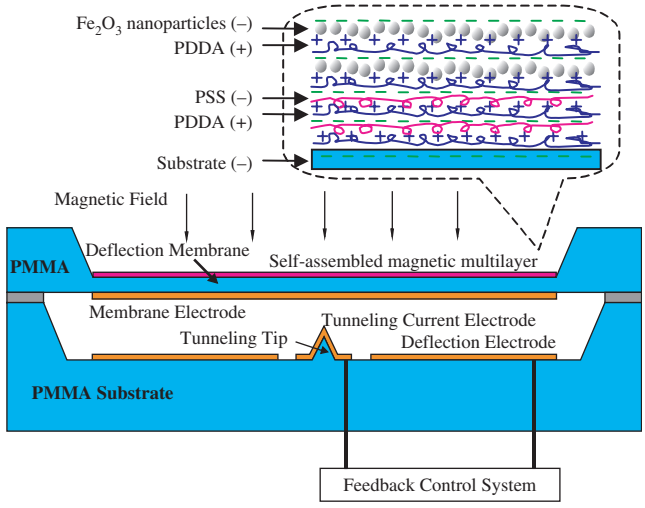

Fig. 1. Schematic structure of the polymer-based tunneling magnetic sensor.

Instead of silicon, polymethylmethacrylate (PMMA) (CYRO Industries ROHAGLAS 99530, thickness: 500 μm, density: 1.15 g/cm^3, Young's Modulus: 2 GPa, Glass transition temperature T_g: 98 °C, melting temperature T_m: 170 °C) is used as the mechanical material. PMMA offers a number of advantages: it is cheap, flexible, optically transparent, and its properties can be modified for specific applications. PMMA has unique thermal and mechanical properties which make it behave ideally in hot embossing process. The spring constant of the membrane, with all edges fixed, can be expressed as:[16]

$$k = \frac{E \cdot t^3}{\alpha \cdot l^2} \tag{1}$$

where E is the Young's modulus, $\alpha = 0.0135$, t and l are the thickness and length of the membrane, respectively. Compared with silicon, PMMA is a "soft" material. Young's moduli of PMMA and silicon are approximately 2 GPa and 165 GPa, respectively. From Eq. (1), the spring constant of the membrane is proportional to E and t^3. For structures with same dimensions, the spring constant of PMMA can be 80 times smaller than silicon. Therefore, when applying the same amount of force on the membranes, the maximum deflection of PMMA structure can be much larger than the silicon structure with the same geometry (thickness, length, etc.). The PMMA structures are more sensitive to external forces. It means that the PMMA structure has the potential to achieve higher sensitivity compared to a silicon structure. In other words, to obtain the same spring constant and sensitivity, a PMMA-based structure can be much thicker than a silicon-based structure. This benefits the design and the fabrication processes.[17]

Among numerous deposition techniques, LbL nano self-assembly is chosen to grow the magnetic layers on the

PMMA surface. Due to its versatility and simplicity, LbL nano self-assembly has gained more and more interest. In LbL self-assembly process, oppositely charged polyions and particles are coated on each other by the electrostatic interaction. This technique has the ability that enables the deposition of nanoparticles, polyions, proteins, DNAs, virus, and other biomolecules onto almost any materials with any topography. Poly(dimethyldiallylammonium chloride) (PDDA) (aqueous solution, MW 200 to 350 K, 3 mg/ml, 0.5 M NaCl, Sigma-Aldrich Co.), poly(sodium 4-styrenesulfonate) (PSS) (aqueous solution, WM 70000, 3 mg/ml, 0.5 M NaCl, Sigma-Aldrich Co.) are used as the polyelectrolytes. Iron oxide particles (Fe_2O_3) (diameter 50 nm), a hard magnetic material suitable for bidirectional actuation,[18] serve as the magnetically sensitive material. Fe_2O_3 nanoparticles are diluted in deionized (DI) water with a final concentration of 2 mg/ml.

2.2. Fabrication

Figure 2 shows the fabrication process of the polymer magnetic actuator. The process starts with the fabrication of the silicon molds (Figs. 2(a–e)). Two silicon molds are required for the subsequent hot embossing process. One silicon mold is for the tunneling tip part; the other mold is for the deflection membrane part. The silicon molds are fabricated with conventional bulk-silicon micromachining techniques. The fabrication of the silicon molds begins with a p-type ⟨100⟩ silicon wafer. Both sides of the silicon wafer are coated with 1 μm SiO_2. A thin layer ($\sim$1.4 μm) of positive photoresist (PR1813) is spin coated on the silicon wafer, and patterned by lithography (Figs. 2(a–b)). Exposed SiO_2 is removed by buffered hydrofluoric acid (BHF) (Fig. 2(c)). Next, the wafer is submerged in a 45% KOH solution. The KOH etchant is kept at 85 °C with a magnetic stirrer rotating at 200 RPM. The etch rate is approximately 0.8 μm/min. The KOH etching is stopped when the silicon pit is formed (Fig. 2(d)). The remaining SiO_2 is removed by BHF etching (Fig. 2(e)).

Hot embossing machines with high precision control of pressure and temperature are now commercially available. HEX 01/LT from Jenoptik Mikrotechnik Company, Germany is used in our project. Hot embossing technique is used to transfer the patterns from the silicon molds to PMMA sheets (Figs. 2(f–g)). For different PMMA structures, the parameters of the hot embossing process need to be modified and optimized. PMMA structures with different sizes have been fabricated. The dimensions of the polymer tunneling tips range from 20 μm × 20 μm to 100 μm × 100 μm. The dimensions of the polymer membranes range from 4 mm × 4 mm to 12 mm × 12 mm. A PMMA sheet is placed in the hot embossing chamber and positioned right below the silicon mold. After evacuating the chamber, the mold is lowered so that it just touches the PMMA sheet. The mold and the PMMA are heated to 165 °C at the same time, a temperature very close to its melting temperature T_m 170 °C in case of uncertainty. Next, the mold is pressed into the PMMA under a contact force of 25 kN. The mold remains pressed for 300 s to ensure that the melted PMMA has sufficient time to flow into the silicon structures and fill in all the cavities. Next, both the mold and the PMMA sheet are cooled down to 80 °C, a temperature lower than its glass transition temperature T_g 98 °C, which provides sufficient strength of the PMMA. The final step is to demold the silicon mold from the PMMA at a speed of 1 mm/min. A typical hot embossing process takes less than 20 min. In addition, a well-fabricated silicon mold with sharp angles and smooth surfaces can be used to reproduce more than 30 PMMA sheets. The complex micromachining process for the fabrication of the silicon molds, normally tens of hours, is only necessarily once. The thickness of the PMMA membrane is reduced by Reactive Ion Etching (RIE). The maximum etch rate on PMMA is approximately 0.5 μm/min when the plasma consists of 2.5% SF_6 and 97.5% O_2.

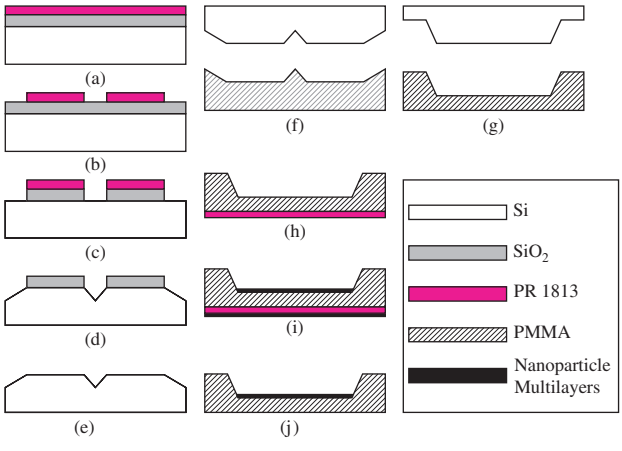

Fig. 2. Fabrication process of polymer magnetic actuator with hot embossing and LbL nano self-assembly.

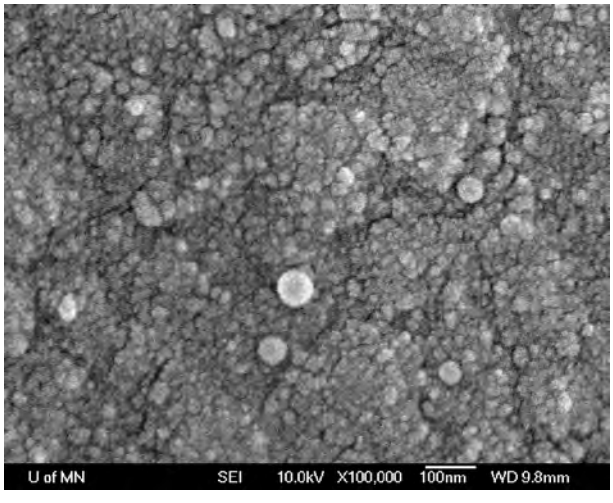

Fig. 3. SEM image of the self-assembled iron oxide (Fe_2O_3) nanoparticle multilayer.

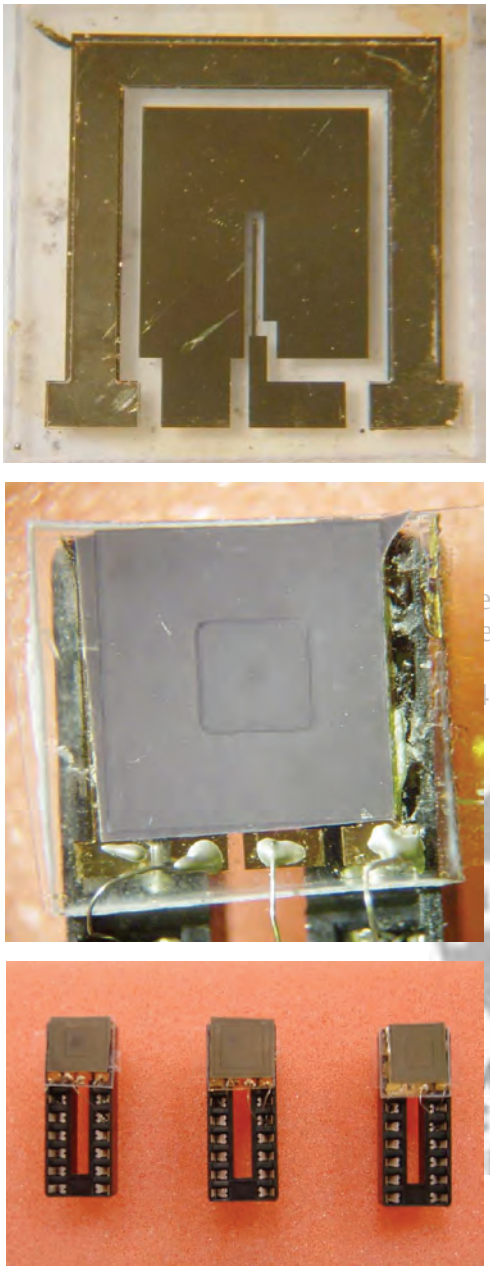

Fig. 4. (a) Optical image of patterned electrodes on PMMA. (b) Assembled PMMA structures. Conductive epoxy is used to bond the two parts together, and connect the copper wires to the gold electrodes. (c) Assembled devices. The devices are mounted on standard 18-pin IC sockets.

Ti/Au (200 Å/1000 Å) films are sputtered on the PMMA structures and patterned as the electrodes.

A layer of positive photoresist (PR1813) is served as the sacrificial layer, which is spin coated on the back side of the membrane to cover the gold electrode. The PR1813 layer is fully exposed under UV light (Fig. 2(h)). The nanoparticle multilayer is coated on the PMMA surface with LbL nano self-assembly. The PMMA membrane is submerged into different solutions, and the sequence of the immersion is: $[\text{PDDA (10 min)} + \text{PSS (10 min)}]_2 + [\text{PDDA (10 min)} + \text{Fe}_2\text{O}_3\text{ (15 min)}]_6$ (Fig. 2(i)). The first four layers of PDDA and PSS are to prepare a smooth base for the subsequent coating. After each immersion, the sample is rinsed in the flow of DI water for 1 min, and then dried using nitrogen stream. Figure 3 shows the scanning electron microscope (SEM) image of the nanoparticle multilayer. Iron oxide nanoparticles with diameter of 50 nm can be clearly seen from the image. The surface of the assembled multilayer is not very smooth because of the RIE dry etching on the PMMA membrane. The rinsing and the drying steps also introduce the non-uniformity of the nanoparticle multilayer. The PR1813 sacrificial layer is stripped off using MF319 solution to uncover the gold electrode (Fig. 2(j)). Two PMMA components are bonded together using conductive epoxy. Copper wires are connected to the gold electrodes using the silver-based conductive epoxy. The whole device is mounted on a standard 18-pin IC socket for testing, as shown in Figure 4.

3. RESULTS AND DISCUSSION

First, the polymer microactuator is tested as an electrostatic actuator. The microactuator can be considered as a parallel capacitor, and the electrostatic force between the two electrodes is proportional to the square of the applied voltage, $F = (\varepsilon A/2g) \cdot V_a^2$, where ε is the permittivity of air, A is the surface area of the electrode, and g is the gap between two electrodes. The membrane deflection amplitude can be express as $d = F/k$, where k is the spring constant of the membrane. Therefore, the deflection of the membrane can be derived as:

$$d = \frac{F}{k} = \frac{\varepsilon \cdot A}{2g \cdot k} \cdot V_a^2 = C \cdot V_a^2 \tag{2}$$

where C is a constant. During the characterization, the membrane electrode voltage is set as the ground. A high periodic signal is applied on the deflection electrode. The membrane oscillates due to the electrostatic force between the electrodes; and deflection amplitude is proportional to V_a^2. A laser interferometer (Polytec VDD 650) is used to detect the small displacement of the oscillated membrane. In our experiment, a 1000 Hz sinusoid wave is applied on the deflection electrode. The voltage is gradually changed from 10 V to 105 V. The deflection amplitudes are recorded by the laser interferometer every 5 V. Figure 5 shows the deflection amplitude of the membrane in response to the applied voltage. The scattered dark squares illustrate the measured data while the line indicates the quadratic polynomial fit as $d = 0.03 \cdot V_a^2$ from Eq. (2). A 20% distortion can be inspected from the figure at higher voltage range ($\geq$100 V). One possible reason is that the devices are assembled by conductive epoxy. The epoxy itself can be compressed during the oscillation of the membrane, especially when the oscillation has high displacement. Moreover, all the devices are manually assembled with the aid of a microscope. The assembling causes some variation and uncertainties.

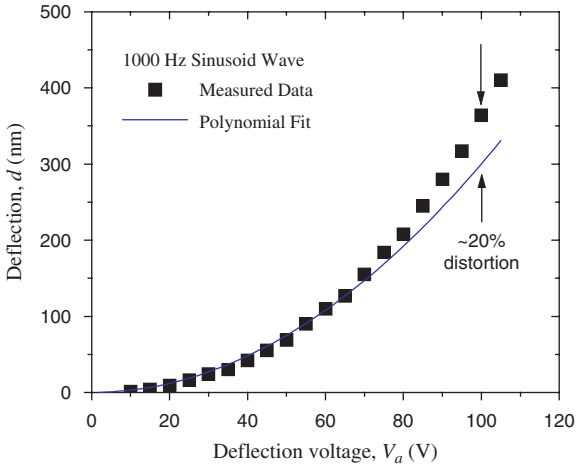

Fig. 5. Measurement of electrostatic force between two electrodes.

From time to time, both dc and ac voltages are required during the operation of the electrostatic actuators. Typically, a high dc voltage is applied to the deflection electrode which is to set the operation point. A small ac voltage, which is caused by the external sensing signal, is added to the dc voltage. The total voltage applied to the membrane is $V_a = V_{DC} + V_{AC}$. The electrostatic force is proportional to $V_a^2 = (V_{DC} + V_{AC})^2 = V_{DC}^2 + 2V_{DC} \cdot V_{AC} + V_{AC}^2$. The first term is a constant value, which is to set the operation point. The other two terms are variable values, which cause the oscillation of the membrane. In dynamic systems, the first term can be neglected.[19] Since $V_{DC} \gg V_{AC}$, the third term can be neglected as well. Only the second term is important and it is linearly proportional to V_{DC}. Therefore, the applied electrostatic force and the detectable oscillation of the membrane are linearly dependent on V_{DC}, $d = R \cdot V_{DC}$. Here we define responsitivity as $R = d/V_{DC}$. The responsitivity of the electrostatic actuator as a function of V_{DC} is shown in Figure 6. The linear relationship is proved and the responsitivity can be extrapolated as $R =$ 0.159 nm/V. During the measurement, the ac component

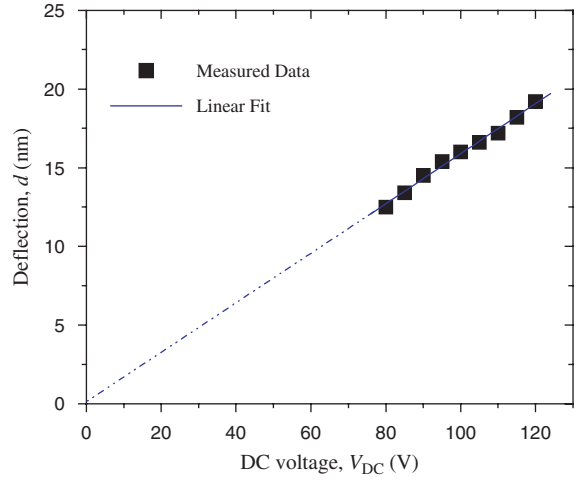

Fig. 6. Dynamic responsivity of the electrostatic actuator.

Table I. Solenoid coil specifications.

Parameters	Values
Dimension	3 cm × 3 cm × 5 cm
Turns	300
Resistance	0.8 Ω
Maximum current	4 A
Inductance	2 mH
Field calculated	7.85×10^{-3} T/A
Field measured[a]	9.50×10^{-3} T/A

[a]A ferromagnetic metal core is inserted.

(1000 Hz sinusoid signal) of deflection voltage is set as 7 V and the dc component is increased gradually from 80 V to 120 V.

With the LbL self-assembled magnetic nanoparticle multilayer, the polymer microactuator is also tested as an electromagnetic actuator. A solenoid coil, which is driven by a sinusoid ac current, is used to produce the magnetic field. The parameters of the solenoid coil and the produced magnetic fields are listed in Table I. A Hall Effect Gaussmeter (model 100) and a probe (model VA-111) are used for field calibration. The vertical electromagnetic force F_z on the magnetic membrane can be expressed as:[20]

$$F_z = M_z \cdot \int_v \frac{dH_z}{dz} dv \tag{3}$$

where M_z, H_z are the vertical components of the magnetization and the magnetic field, respectively. v is the volume of the magnet, the magnetic multilayer in our case. From the equation, the electromagnetic force is proportional to the volume of the magnet. Therefore, deposition methods that can accurately control the magnet volumes are preferred. Commonly used magnet deposition methods include glue bonding, spin casting, electroplating, screen printing, etc. However, the thickness of the magnet can only be controlled in millimeter or micron scale based on these techniques. By using the LbL self-assembly, the magnet volume can be precisely controlled by the number of Fe_2O_3 layers in nanometer accuracy.

To determine the natural frequency of the microactuator, ac signals ranging from 25 Hz to 6 kHz are applied to the solenoid coil. Under the influence of the magnetic field generated by the solenoid coil, the PMMA membrane vibrates accordingly. Figure 7 shows the deflection amplitude as a function of the driven frequency. The size of the membrane is 10 mm × 10 mm, the thickness is approximately 10 μm. Six layers of Fe_2O_3 nanoparticles are self-assembled on the membrane. The natural frequency of the device is approximately 151 Hz and at this point the deflection amplitude reaches 34 nm. The natural frequency of a square-shaped membrane with all edge fixed can be expressed as:[16]

$$f = \frac{K_1}{2\pi} \sqrt{\frac{E}{12(1-\gamma^2)\rho}} \tag{4}$$

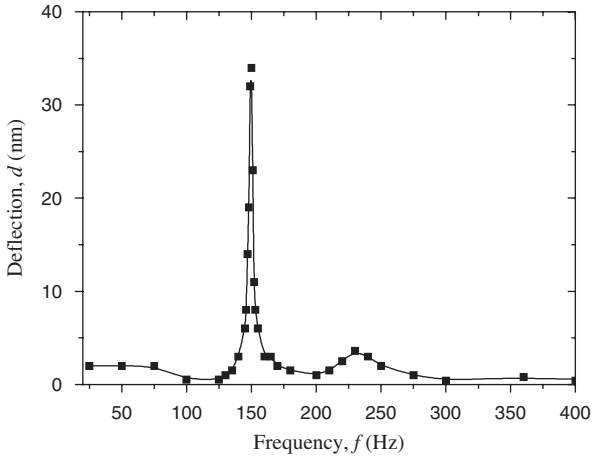

Fig. 7. Frequency response of the polymer magnetic actuator.

where $K_1 = 36$, $E = 2$ GPa, $\gamma = 0.4$, $\rho = 1.15$ g/cm^3 are Young's modulus, Poisson's ratio, and density of PMMA, respectively. Based on Eq. (4), the natural frequency of a membrane with dimension of 10 mm × 10 mm × 10 μm can be calculated as 238 Hz, which is 57.6% higher than the measured value 151 Hz. The difference between the measured and the calculated values comes from two sources. As shown in Figure 1, the top PMMA part consists of a membrane and some area bonded to the bottom PMMA substrate. However, due to the uncertainty of the manual assembly, part of the bonded area is not firmly glued to the substrate. It increases the actual membrane area during the measurement. Theoretically, a membrane with dimension of 12 mm × 12 mm × 10 μm has a natural frequency of 165 Hz, which is very close to our measured result. The other reason comes from the non-uniformity of the membrane. The PMMA thickness is reduced by RIE dry etching. As inspected by SEM, the RIE etched surface is not very smooth. The average thickness of the membrane could be slightly less than 10 μm. The non-uniformity of the membrane affects the measured results.

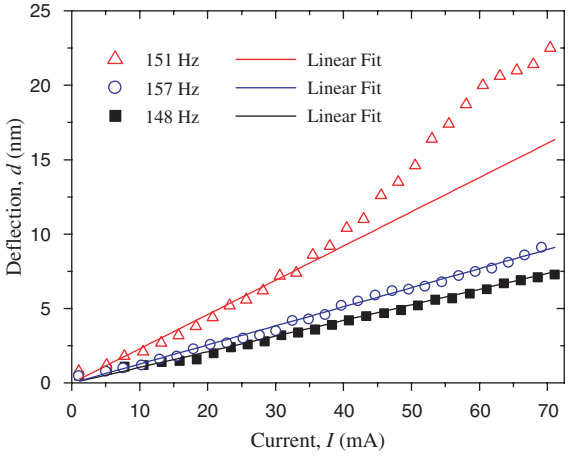

Fig. 8. The deflection amplitude versus the applied current.

The deflection of the membrane is measured as a function of the applied ac current through the solenoid coil. Based on equation: $B = \mu \cdot n \cdot I$ (where μ, n, I represent the permeability, turn density, and current of the solenoid coil, respectively), the generated magnetic field is proportional to the applied ac current. From Eq. (2) and (3), the deflection d is linearly proportional to the applied ac current at all frequencies. The deflection amplitudes as functions of the currents at three difference frequencies (from top to bottom, 151 Hz, 158 Hz, and 148 Hz) are shown in Figure 8. The membrane has the maximum deflection amplitude at its nature frequency 151 Hz. The linear fits (solid lines) of these data are also shown in the figure. The linear functions are $d = 0.230 \cdot I$, $0.128 \cdot I$, and $0.105 \cdot I$, respectively. As for 148 Hz and 157 Hz signals, the linear fits match the measured data perfectly from 0 to as high as 70 mA. However, for the 151 Hz signal, the linear fit can only match the measured data up to 40 mA. Relatively large errors are recorded from 40 mA to 70 mA. Again, the possible reasons are the compressed conductive epoxy during large deflection and the manual assembly.

4. CONCLUSIONS

This paper shows the design, fabrication, and characterization of a low-cost polymer-based magnetic microactuator. The actuator was fabricated with hot embossing technique and LbL nano self-assembly. Using hot embossing technique and PMMA, an inexpensive polymer, low-cost devices with massive and rapid replication can be produced. LbL nano self-assembly was chosen to coat the magnetic layers on the PMMA surface due to its simplicity and the ability that enables the deposition of nanoparticles onto almost any material. The coating sequence was: [PDDA (10 min) + PSS (10 min)]$_2$ + [PDDA (10 min) + Fe_2O_3 (15 min)]$_6$. PDDA and PSS were used to prepare a smooth base for the subsequent coating. Iron oxide nanoparticles were used as the magnetically responsive material. Totally there are 6 layers of Fe_2O_3 coated on the membrane. The volume of the magnetic material can be precisely controlled by the number of the assembled Fe_2O_3 layers. The device was assembled using a conductive epoxy, and then mounted on the standard IC sockets. A solenoid coil was used to generate the magnetic field which can oscillate the PMMA membrane. The displacement of the membrane was detected by a laser interferometer. The natural frequency and the deflection amplitude of the polymer magnetic microactuator were measured and analyzed. To improve the performance and stability of the PMMA-based devices, assembly and packaging should be modified and optimized. Automated, or semi-automated, machine assembly and packaging are believed to be able to reduce the uncertainties greatly. Compared with silicon or glass-based devices, polymer-based devices typically have lower stability and lower temperature endurance. However,

due to the inherent advantages such as lower cost, faster fabrication, better chemical and biological compatibility, and higher sensitivity, polymer-based devices have the potential abilities for a wide range of applications.

References and Notes

1. L. K. Lagorce, O. Brand, and M. G. Allen, *J. Microelectromech. Syst.* 8, 2 **(1999)**.
2. J. W. Judy and R. S. Muller, *J. Microelectromech. Syst.* 6, 249 **(1997)**.
3. W. P. Taylor, M. Schneider, H. Baltes, and M. G. Allen, *Proceeding of Transducers'97*, Chicago, IL, 1445, **(1997)**.
4. J. W. Judy, R. S. Muller, and H. H. Zappe, *J. Microelectromech. Syst.* 4, 162 **(1995)**.
5. L. K. Lagorce and M. G. Allen, *Proceeding of IEEE MEMS'96*, San Diego, CA, 85 **(1996)**.
6. Yingguo Peng, Chando Park, and D. E. Laughlin, *J. Appl. Phys.* 93, 7957 **(2003)**.
7. I. J. Busch-Vishniac, *Sens. Actuat. A-Phys.* 33, 207 **(1992)**.
8. L. K. Lagorce and M. G. Allen, *J. Microelectromech. Syst.* 6, 307 **(1997)**.
9. H. Miyajima, N. Asaoka, M. Arima, Y. Minamoto, K. Murakami, K. Tokuda, and K. Matsumoto, *J. Microelectromech. Syst.* 10, 418 **(2001)**.
10. K. Pfeiffer, M. Fink, G. Ahrens, G. Gruetzner, F. Reuther, J. Seekamp, S. Zankovych, C. M. Sotomayor Torres, I. Maximov, M. Beck, M. Graczyk, L. Montelius, H. Schulz, H.-C. Scheer, and F. Steingrueber, *Microelectron. Eng.* 61–62, 393 **(2002)**.
11. Joseph Wang, Martin Pumera, and Madhu Prakash Chatrathi, *Electrophoresis* 23, 596 **(2002)**.
12. F. Hua, T. Cui, and Y. Lvov, *Langmuir* 18, 6712 **(2002)**.
13. F. Hua, J. Shi, Y. Lvov, and T. Cui, *Nano Lett.* 2, 1219 **(2002)**.
14. C. H. Liu and T. W. Kenny, *J. Microelectromech. Syst.* 10, 425 **(2001)**.
15. H. Schift, L. J. Heyderman, M. Auf der Maur, and J. Gobrecht, *Nanotechnology* 12, 173 **(2001)**.
16. W. C. Young, Roark's Formulas for Stress and Strain, 6th edn., McGraw-Hill, New York **(1989)**.
17. W. Xue, J. Wang, and T. Cui, *IEEE/ASME T. Mech.* 10, 468 **(2005)**.
18. H. J. Chao and C. H. Ahn, *J. Microelectromech. Syst.* 11, 78 **(2002)**.
19. C. H. Liu, A. M. Barzilai, J. K. Reynolds, A. Patridge, T. W. Kenny, J. D. Grade, and H. K. Rockstad, *J. Microelectromech. Syst.* 7, 235 **(1998)**.
20. B. Wagner, W. Benecke, G. Engelmann, and J. Simon, *Sensor. Actuat. A-Phys.* 32, 598 **(1992)**.

Received: 5 June 2006. Accepted: 5 December 2006.